International Journal of Gas Turbine, Propulsion and Power Systems
October 2014, Volume 6, Number 2

Prediction of Effects of Potential Field Interaction and Wake Interaction on Unsteady Force for Buckets

Tomomi Nakajima[1], Yoshio Shikano[2] and Yutaka Yamashita[2]

[1] Hitachi Research Laboratory, Hitachi, Ltd.*
3-1-1 Saiwai-cho, Hitachi-shi, Ibaraki 317-0073, JAPAN
E-mail: tomomi_nakajima@mhps.com
[2] Hitachi Research Laboratory, Hitachi, Ltd.*

ABSTRACT

This paper describes the unsteady force acting on steam turbine buckets which is induced by a potential field and a wake. A new method is proposed that can separate a potential field interaction and a wake interaction from the unsteady viscous flow computation. The new method does two computations for one model to get inviscid and viscous flow solutions. Then the quantitative effects of the factors that influence the unsteady force acting on the turbine buckets are clarified.

The nozzle-bucket axial gap length is adopted for the factor to be studied and the proposed method is used to calculate the unsteady force of the bucket sections with different bucket heights in the same stage. The simple relationships between the nozzle-bucket axial gap length and the unsteady force are found to give easy and reliable prediction of the force.

INTRODUCTION

For turbine buckets, resonance by the unsteady force which is induced by cascade interaction becomes spoil the safety of the buckets. This is known as the NPF (nozzle passing frequency) excitation. This excitation frequency is a value in which the number of nozzles is multiplied by rotational speed and harmonic contents. The unsteady force has complex effects due to a potential field interaction and a wake interaction. The potential field interaction is an inviscid interaction due to time variation of the pressure field and it is induced by time variation of the relative position of a nozzle and the buckets. The wake interaction gives the flow field an unsteady nature for the boundary layer and vortex, and it also gives a wake from the upstream cascade, which causes pressure fluctuation on the surface of the bucket.

Factors such as the bucket profile and nozzle-bucket axial gap length influence the unsteady force. The relationships between unsteady force and these factors are very complicated, so a direct solution by computational fluid dynamics (CFD) is generally used to obtain the unsteady force acting on the turbine buckets. But it is difficult to get a quantitative effect of each factor independently using CFD, so it is difficult to analyze the unsteady force with the factors. The main reason for the latter difficulty is that the unsteady force is made up of a potential field interaction and a wake interaction. To identify the mechanism of the unsteady force, a scheme that can evaluate the effect for each interaction is important.

Many examples of a direct solution for the unsteady force by CFD have been published (see e.g., [1, 2]). Lan et al.[1] carried out a 3-dimensional numerical simulation of the unsteady flow across the one-and-a-half stage axial turbine with different mass flow cases. They clearly saw that the unsteady aerodynamic force on the blade was changed at different mass flows from the design case. Praisner et al.[2] presented 3-dimensional computational results of closely coupled high and low pressure turbines in both co- and counter-rotating configurations with a focus on the prediction of the unsteady loading for the first blade of the low pressure turbine. The peak-to-peak amplitude of the tangential load was varied compared to the co-rotating 3-row and 4-row results. Generalization of the unsteady force has also been well studied. Kemp and Sears[3] applied an analysis scheme of the unsteady force for a no-camber thin blade and their work was followed by other studies for compressor cascades, for example [4, 5]. Osborne[4] performed approximate calculations for the problem of the unsteady aerodynamic interference between two cascades of 2-dimensional airfoils with relative motion in subsonic compressible flow. He found closed-form formulas for the forces, for the potential interactions (including the rotor vortex-wake interactions) and for the viscous-wake interactions. Naumann and Yeh[5] considered the unsteady lift of a flat-plate and extended the analysis to cambered airfoils with an angle of attack moving through both longitudinal and transverse gusts. But Nishiyama and Funazaki[6] made it clear that the assumption Kemp and Sears used for their scheme did not work for large steady load blades such as turbine buckets.

There are a few reports on the splitting of the potential field interaction and the wake interaction. Korakianitis[7, 8] showed the amplitudes and phases of the unsteady force quantitatively, those of the potential field interaction and wake interaction independently, and the contribution of both interactions. He surveyed the axial gap between the nozzle and bucket and their pitch ratio and showed that the amplitude and phase of the unsteady force which was for only one interaction changed simply for the factors, but changed complexly for the combined interaction. He also found an optimum axial gap where vortical and potential excitation effects were partially cancelled out. Feiereisen et al.[9] used two methods to split the measured gusts into vortical and potential components for experimental data. The split theory by Goldstein[10] considered inviscid compressible flow and it could be calculated as if the body had zero thickness and zero angle of attack. Jocker et al [11] also used the split theory for a 2-dimensional subsonic turbine stage with extremely large blade loads. They investigated the effects of parameters such as the axial gap, stator pitch and stator size. They found that when potential and vortical excitations were the same magnitude, phase turning of the effects could result in a minimized excitation. Hoyningen-Huene and Hermeler[12] presented a numerical 2-dimensional study of the unsteady flow in the first stage

* Mitsubishi Hitachi Power Systems, Ltd. since Feb. 2014

Presented at International Gas Turbine Congress 2011 Osaka, November 13-18, Osaka, Japan, IGTC2011-053
Review Completed on May 30, 2014

of an industrial axial flow gas turbine, especially focusing on the influence of axial spacings. They investigated the effects of the potential flow interaction and wake-blade interaction for the magnitude and phase of the unsteady force. For design engineers, they set the design criterion using only geometrical stage data that helps engineers in determining axial gaps by taking into account the fluctuation amplitudes of both rotor incidence and static pressure fluctuation in the rotor leading edge region.

But no reports have evaluated quantitative effects for each interaction and no schemes have been presented that can split the effects from the unsteady force into the potential field interaction and the wake interaction and then can evaluate the individual effects. The purpose of this paper is to explain the method for generalization of the unsteady force by splitting, evaluating and combining effects of these two interactions. Results obtained by applying this method to the steam turbine bucket are also presented.

NOMENCLATURE

A	amplitude [N/m]
a	first coefficient of exponential function [-]
B1	periodic condition boundary [-]
B2	connecting boundary [-]
b	second coefficient of exponential function [-]
C	chord length [mm]
Cw	axial chord length [mm]
d	nozzle-bucket axial gap length (between nozzle trailing edge and bucket leading edge) [mm]
F	force [N/m]
FA	axial force [N/m]
FT	tangential force [N/m]
h	section height [%]
i	intercept of the phase line[-]
IP	intermediate pressure [-]
j	phase when unsteady force is the maximum [deg]
k	gradient of the phase line[-]
L	tangential length of computational model [mm]
LE	leading edge [-]
m	first coefficient of power function [-]
N	blade number [-]
n	second coefficient of power function [-]
P	pressure [Pa]
s	throat [mm]
T	pitch [mm]
TE	trailing edge [-]
t	time or nozzle passing period [-]
ta	turning angle [deg]
α	outlet angle of nozzle [deg]
β	inlet angle of bucket [deg]
γ	outlet angle of bucket [deg]
ω	angular velocity [rad/s]
θ	phase [deg]

Subscripts

b	bucket
mean	mean pressure
n	nozzle
p	potential field interaction component
total	inlet total pressure
w	wake interaction component

NUMERICAL APPROACH

Computational Method

Reynolds averaged Navier-Stokes equations are solved for an unsteady compressible flow field using a finite volume method and multi-domain technique. To stabilize the computation, the approximate Rieman solver proposed by Roe[13] is introduced for the convection term calculation. The Adams-Bashforth method of second-order accuracy, which is an explicit method, is used for the time integration. The ideal gas equation of state is employed to relate pressure and temperature and Sutherland's equation is introduced to calculate molecular viscosity. In the present analysis, the two-equation model of turbulence proposed by Chien[14] is used to compute a turbulence effect. To compute the flow field shown in Fig.1, boundary conditions are set as follows. Total pressure, total temperature and flow direction are specified at the inlet boundary of the nozzle flow field and a static pressure is specified at the outlet boundary of the bucket flow field. At the boundary B1, the periodic condition is introduced. On the blade surface, the velocity components are set equal to zero and the adiabatic condition is also applied. For the transport equation of turbulence, the wall function method proposed by Launder and Spalding[15] is introduced to reduce computing time. The last boundary is the connecting boundary B2; it is where the data transfer is carried out between the nozzle and bucket flow regions considering the moving bucket location at each time step of the calculation.

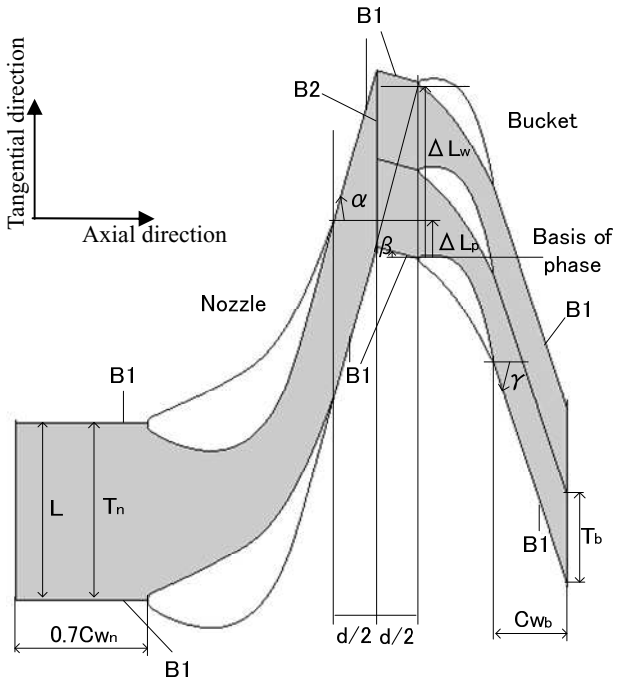

Fig. 1 Description of investigated turbine stage configuration

In this study, the linear interpolation technique is employed considering a connecting boundary mesh location at each time step. Computational models are created which have nozzle inflow parts of $0.7Cw_n$ and bucket outflow parts of Cw_b.

The bucket surface pressure obtained by CFD is used to calculate the tangential force (FT) and the axial force (FA). In Fig.1, the bucket area and the nozzle area are connected by B2, and the line from the nozzle trailing edge has the gradient of the nozzle outlet angle and the line from the bucket leading edge has the gradient of the bucket inlet angle. The positional condition in the figure is defined as t=0.0, the basis of the phase of all forces.

ΔL_p and ΔL_w shown in Fig.1 are the tangential distances calculated as follows.

$$\Delta L_p = T_n - \frac{d}{2} \times (\tan\alpha + \tan\beta) \quad (1)$$

$$\Delta L_w = \frac{d}{2} \times (\tan\alpha - \tan\beta) \quad (2)$$

Here, ΔL_p is the moving distance from the position t=0.0 until the bucket leading edge is nearest the nozzle trailing edge in the axial direction, and ΔL_w is the geometrical distance from the position

Table 1 Design point data

Item	Unit	Value
Rotational Speed	(rpm)	3000
Inlet Total Pressure	(kPa)	1337
Inlet Total Temperature	(K)	695
Outlet Static Pressure	(kPa)	1109

Table 2 Test case data

Case No	h (%)	ta (deg)	α (deg)	β (deg)	γ (deg)	C_n (mm)	C_b (mm)	T_n (mm)	T_b (mm)
1	100	30.0	72.3	-45.6	75.6	115.5	50.0	76.2	38.1
2	46.6	56.2	74.1	-15.5	71.7	105.8	50.0	69.8	34.9
3	0	117.1	75.1	49.4	67.7	92.2	50.0	60.8	30.4

t=0.0 until the bucket leading edge arrives at the centre of the wake.

Computations are carried out for an actual steam turbine stage with the conditions as listed in Table 1. Three places in the bucket section, the root, near the mid span, and the tip are targeted (see Table 2), and cascades are created to get six nozzle-bucket axial gap lengths. The axial gap length is varied between 5 % and 40 % of the nozzle chord. The ratio of the number of buckets to the number of the nozzles, N_b/N_n, which has a large influence on the unsteady force (see e.g., [7, 8, 11]), is set to 2 (N_b=2, N_n=1). The computational model is made by design s/T, so the pitch becomes large when h becomes large, and the nozzle chord length becomes large in proportion to the ratio of pitch, too. In this study, the bucket chord length is fixed at 50 mm so that it does not depend on h. For the calculation, the bucket moving speed is set at the speed at which the bucket incidence angle is 0 degree for a viscous flow solution. Only the first harmonic unsteady force, as the nozzle passing frequency component, is considered, so the amplitude and the phase described later are also for the first harmonic.

Generalization Method

To develop the method for generalizing the unsteady force, it is assumed that the unsteady force is combined with two effects, the potential field interaction and the wake interaction. For this assumption, the unsteady force F(t) can be expressed by Eq. (3).

$$F(t) = A\sin(\omega t + \theta) = A_p \sin(\omega t + \theta_p) + A_w \sin(\omega t + \theta_w) = F_p(t) + F_w(t) \quad (3)$$

The proposed method does two computations for one model to get inviscid and viscous flow solutions. The unsteady Reynolds average Navier-Stokes (U-RANS) solver is used to compute the viscous flow field. The unsteady force acting on the bucket obtained from the U-RANS consists of effects of both potential field and wake interactions. For the unsteady inviscid flow (Euler) solution, using a sharply pointed shape (cusp) for the nozzle trailing edge instead of the actual round shape is the key to restraining the dummy wake generation (Fig.2). Then only the potential field interaction can be obtained. A linear relation between the potential field and wake interactions is assumed and the unsteady force induced by the wake interaction is obtained by subtracting Euler's aero-dynamic force from that of the U-RANS. After two computations, the amplitude and the phase of the unsteady force are obtained by Eqs. (4) and (5).

$$A = \sqrt{\{A_p \cos\theta_p + A_w \cos\theta_w\}^2 + \{A_p \sin\theta_p + A_w \sin\theta_w\}^2} \quad (4)$$

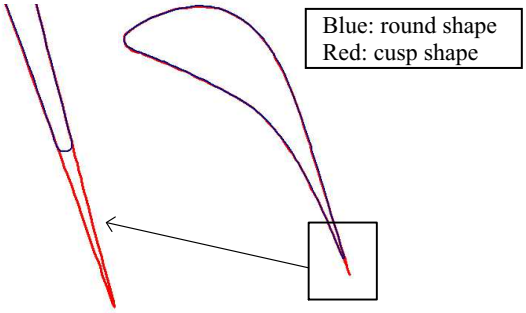

Fig. 2 Nozzle section trailing edge (cusp and round shapes)

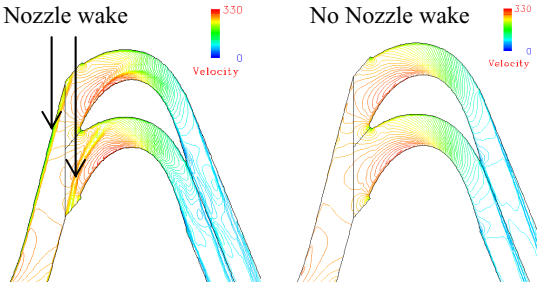

(a) Viscous flow field (b) Inviscid flow field

Fig. 3 Instantaneous velocity flow fields for case3, d/C_n=0.15

$$\theta = \tan^{-1}\{(A_p \sin\theta_p + A_w \sin\theta_w)/(A_p \cos\theta_p + A_w \cos\theta_w)\} \quad (5)$$

The amplitude and the phase of the effects of potential field and wake interactions can be expressed as a function of axial gap length. The unsteady force for an arbitrary axial gap length can be predicted by making the numerical formula.

Instantaneous velocity flow fields for inviscid and viscous flow solutions are shown in Fig.3. A wake generated from the nozzle trailing edge is observed only for the viscous flow field. This finding indicates that the influence of the wake can be excluded in the inviscid flow solution.

RESULTS

Figure 4 provides the results of the survey about the unsteady force and axial gap length d/C_n. Generally, the amplitude A becomes large when the axial gap length becomes small, but the trend is different for FT and FA of case 1, and FA of case 3, and the unsteady force does not monotonously change according to d/C_n. In cases 1 and 2, d/C_n values which give amplitude A the local maximum and local minimum values are close for FT and FA, and the changes in the phase for d/C_n values are almost the same. But in case 3, FT and FA change in almost opposite ways and the changes in the phase for d/C_n do not look at all similar. As seen above, the amplitude and the phase of the unsteady force have different behaviours for d/C_n according to the bucket height h and FT and FA, and the trend in the amplitude of the unsteady force is numerically complicated.

Figure 5 plots the amplitudes and phases of the potential field and wake interactions, which are obtained by inviscid and viscous flow solutions. When the effect of each interaction is obtained individually, the amplitude becomes large when d/C_n becomes small. The amplitude of the potential field interaction can be approximated by an exponential function of d/C_n, while the

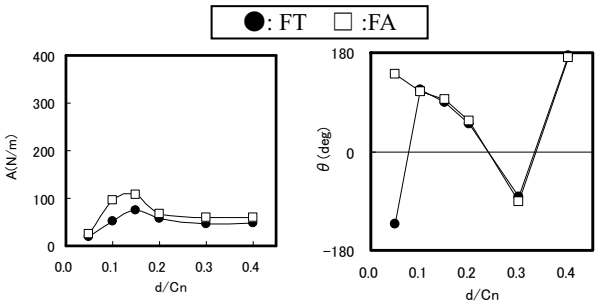

(a) Case 1: h=100%

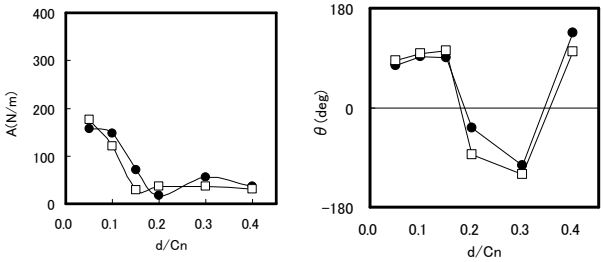

(b) Case 2: h=46.6%

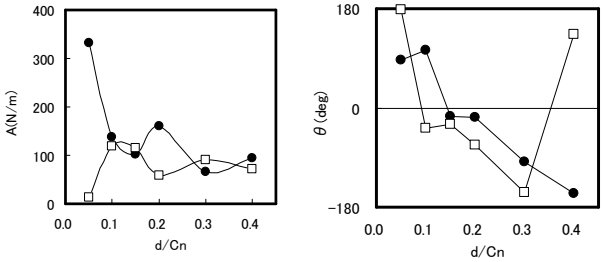

(c) Case 3: h=0%

Fig. 4 Amplitudes and phases of unsteady force 1st harmonic

amplitude of the wake interaction can be approximated by a power function of d/C_n, for both FT and FA. The coefficients of these approximate expressions differ according to the bucket height h and FT and FA. Thus the amplitude of each interaction should be given by an expression under each condition.

Next, the phase is considered. The phase of each interaction has a linear relationship with d/C_n. The gradients of these lines of the phase are almost the same in each case, then they do not depend on FT and FA, and this agrees with values obtained by Eqs. (1) and (2). Therefore the line of the phase is expressed by Eq. (6):

$$\theta = k \cdot \frac{d}{C_n} + i \qquad (6)$$

where k and i are the gradient and the intercept of the linear function of the phase of each interaction, respectively. In Fig.5, the vertical axis of the phase graphs is plotted with a larger scale than that of Fig.4 to make a point of showing that the phase changes on a straight line for d/C_n. If it is considered that a cycle includes angles from 0 to 360 degree, the values of 360 integral multiples are equal.

An example of the fluctuation of the bucket force is shown in Fig.6 (case 3, FA). The black line plots the fluctuation of the unsteady force that is obtained by a viscous flow solution. The red line plots the fluctuation of the force of the potential field interaction that is obtained by an inviscid flow solution. The blue line plots the fluctuation of the force of the wake interaction that is obtained by Eq. (3). Figure 6 has the same trend as Fig.5 that the amplitude of each interaction becomes big when d/C_n is small.

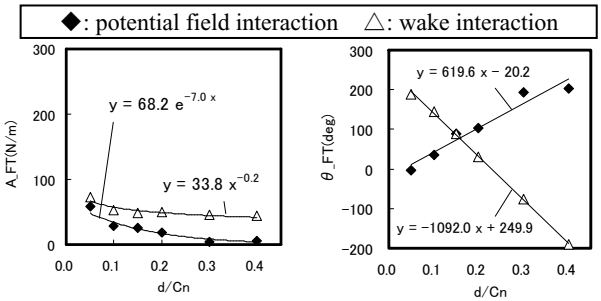

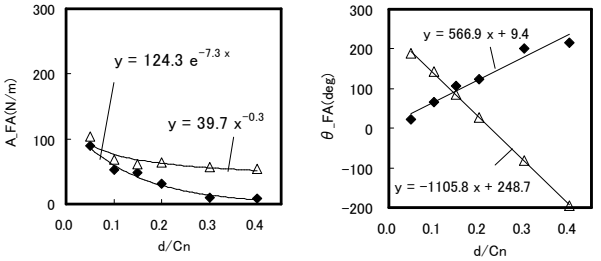

(a) Case 1: h=100%

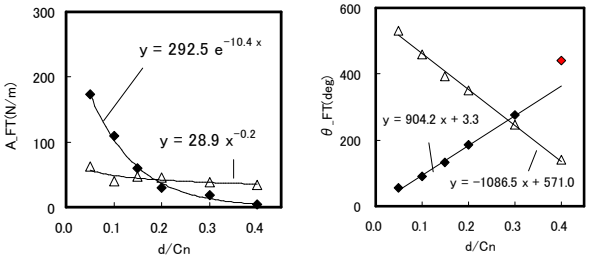

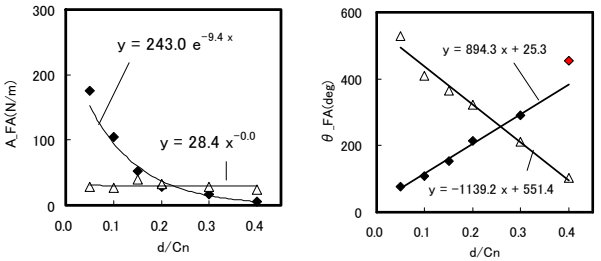

(b) Case 2: h=46.6%

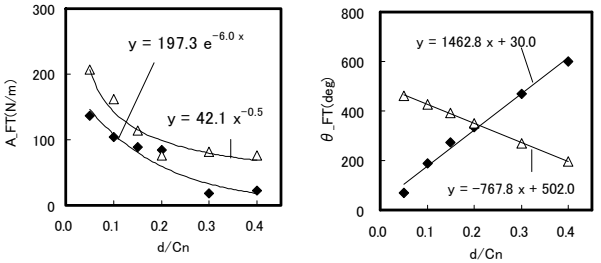

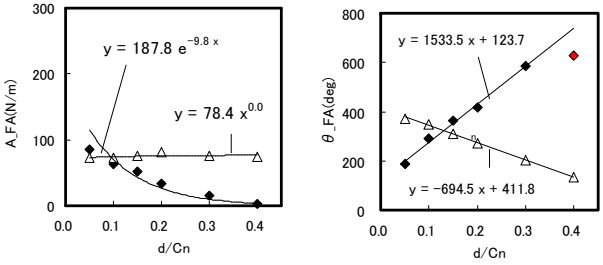

(c) Case 3: h=0%

Fig. 5 Amplitudes and phases of effects of potential field interaction and wake interaction

However, the amplitude of the unsteady force is small when d/C_n is small. This depends on the phase relations of the potential field and the wake interactions. Figure 6 shows that the phase of each interaction is approximately opposite for d/C_n=0.05 and that it is approximately the same for d/C_n=0.15. So it is revealed that the phase relations of the potential field interaction and the wake interaction have a strong influence on the size of the amplitude of the unsteady force.

The effect of the potential field interaction depends on the bucket moving distance ΔL_p where the nozzle trailing edge and the bucket leading edge approach each other axially, and the variation of the phase to d/C_n is equal to the variation of ΔL_p. The effect of the wake interaction depends on the bucket moving distance ΔL_w which relates to a straight line length that extends from the nozzle trailing edge to the bucket leading edge in the direction of the nozzle outlet flow angle, and the variation of the phase to d/C_n is equal to the variation of ΔL_w. Table 3 shows the gradients of each interaction obtained from ΔL_p and ΔL_w. In this paper, it is assumed that the gradient of the linear function of the phase is known from Table 3, and importance is attached to obtaining the intercept which is difficult to predict from a geometrical size by using Fig.5. Therefore, all points which lead to a greatly different gradient from that of Table 3 are not used to predict the phase (red marks in Fig.5). The amplitudes of the excluded data are small, so it likely that the phase was not calculated accurately. Figure 5 shows that the intercepts obtained from CFD data differ according to bucket height h, and a simple relation between intercept and h or ΔL_p, ΔL_w cannot be found, though ΔL_p and ΔL_w are considered generally to be tangential distances that enlarge the effect of each interaction the most. This is the cause of the difference of bucket shape according to bucket height h which leads to the difference at the time when the change in the fluctuating pressure on the bucket surface becomes the maximum. This phenomenon can be seen in the pressure distribution shown in Fig.7 where the contour is $(P-P_{mean})/P_{total}$. FT can be evaluated using Fig.7. The graphs which are written as "V" are the results of the viscous flow solutions, and the graphs which are written as "I" are the results of the inviscid flow solutions. The graph "V" shows the potential field and the wake interactions, and the "I" shows only the potential field interaction. Figure 7 "V" shows t obtained from ΔL_w (blue straight line), and it is in the vicinity of t where the wake is seen (oval part shown with the dashed line), and it is understood to be related to both t values. But both t values are not related to t for which the effect of the wake

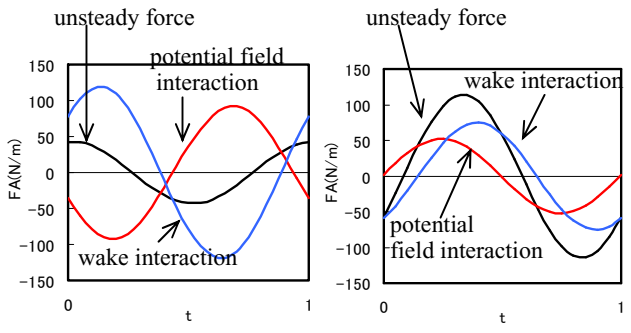

(a) d/C_n=0.05 (b) d/C_n=0.15

Fig. 6 Bucket force fluctuation (Case 3, FA)

Table 3 Gradient k obtained from ΔL_p and ΔL_w

Interaction ＼ Case No	Case 1	Case 2	Case 3
Potential Field Interaction	607.7	882.6	1408.3
Wake Interaction	-1193.2	-1084.6	-739.4

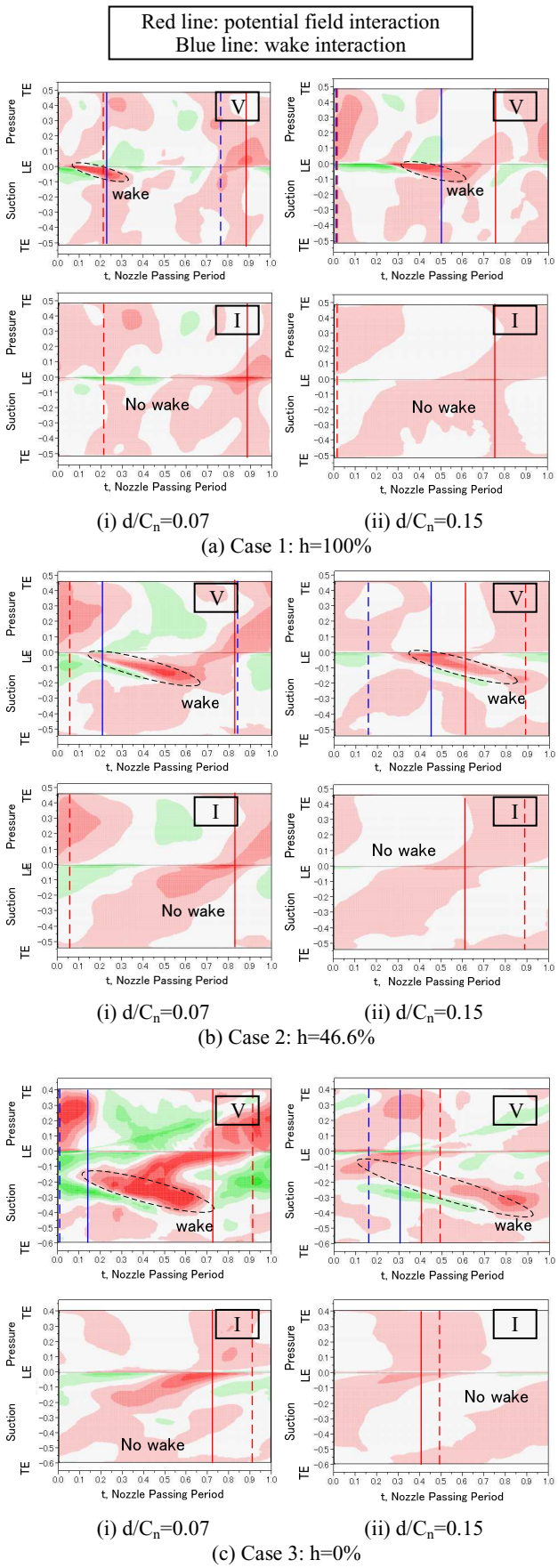

(i) d/C_n=0.07 (ii) d/C_n=0.15

(a) Case 1: h=100%

(i) d/C_n=0.07 (ii) d/C_n=0.15

(b) Case 2: h=46.6%

(i) d/C_n=0.07 (ii) d/C_n=0.15

(c) Case 3: h=0%

Fig. 7 Time-space plots of bucket surface perturbation pressure, V=Viscous, I=Inviscid

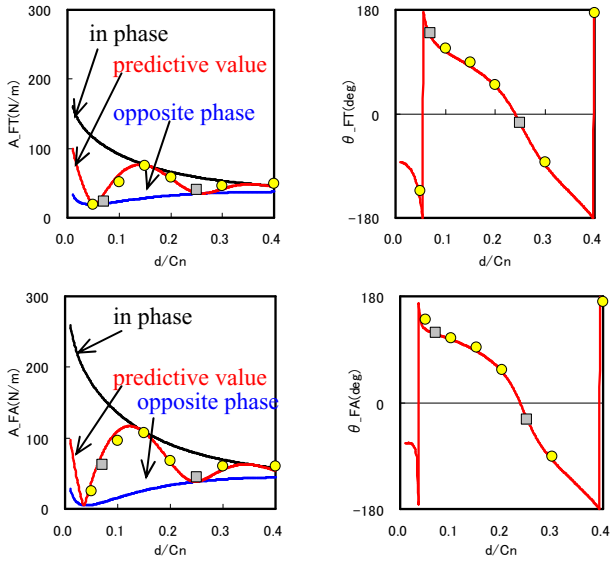

(a) Case 1: h=100%

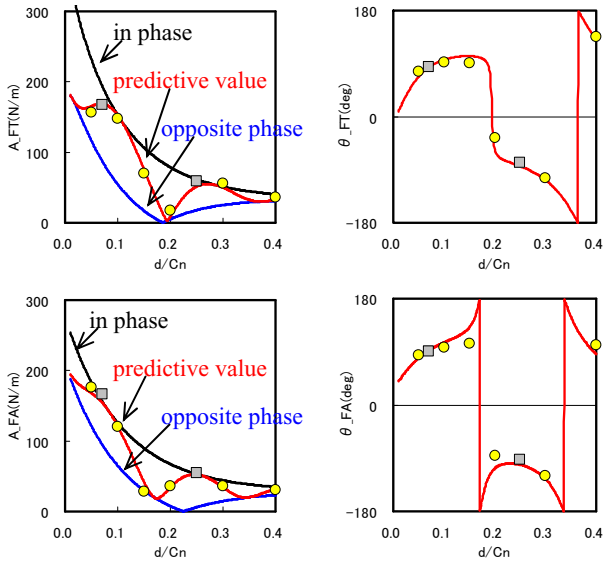

(b) Case 2: h=46.6%

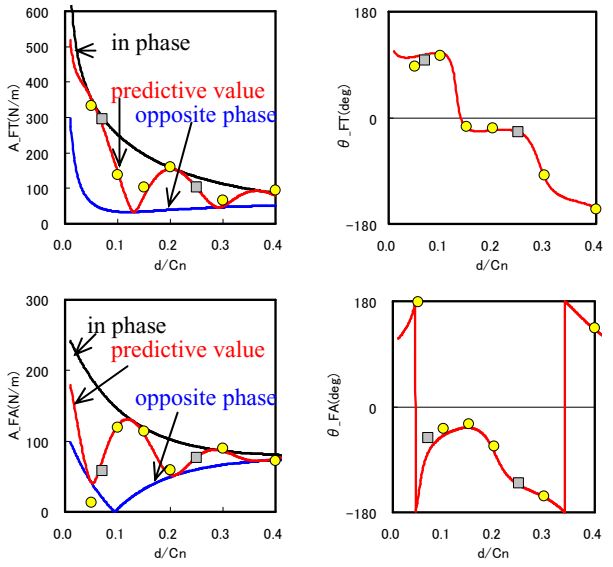

(c) Case 3: h=0%

Fig. 8 Predictive amplitudes and phases of unsteady force

interaction becomes strongest (Fig.7 "V" blue dashed line) obtained from Fig.5. The same is true about the potential field interaction (red line). Figure 7 "I" shows t obtained from ΔL_p (red straight line), and it is in the vicinity of t where the pressure fluctuation at the leading edge is maximum, and it is understood to be related to both t values. But both t values are not related to t for which the effect of the potential field interaction becomes strongest (Fig.7 "I" red dashed line) obtained from Fig.5. Thus it is clear that prediction of the intercept of the phase is not easy. But the difference between t obtained from ΔL (straight line) and t obtained from the result of CFD (dashed line) is approximately equal, not depend on d/C_n and bucket height h. Thus the intercept of the phase is equal when the basis of the phase is set to ΔL, if d/C_n is changed. So the intercept can be obtained by one solution.

The amplitude and phase of the unsteady force are obtained by Eqs. (4) and (5), using the amplitude and the phase of each interaction shown in Fig.5. These results are presented in Fig.8. The black lines plot the results which are obtained assuming that the phase of the potential field interaction and the phase of the wake interaction are the same, so this value is the sum of the amplitudes of the two interactions, A_p and A_w. The blue lines plot the results which are obtained assuming that the phase of the potential field interaction and the phase of the wake interaction are opposite: therefore this value is an absolute value of the difference between A_p and A_w. The obtained predictive values (red line) change between the black and blue lines according to the difference of the phase of each interaction. Therefore, there is a clear possibility of not evaluating quantitatively the unsteady force if the phase of each interaction is not considered. The ○ marks in Fig.8 are the results shown in Fig.5, and the data used to make the expression to predict the unsteady force. The □ marks in Fig.8 are additional data calculated by CFD to evaluate the expression to predict the unsteady force, for d/C_n=0.07, 0.25. Figure 8 shows that the line for the predictive values (red line) and the ○ and □ are in good agreement with each other, for both the amplitude and the phase. Regarding the difference between the predictive values and the values calculated with CFD (shown with □), for the amplitude, the maximum is 15 N/m and the average is 7.3 N/m, and for the phase, the maximum is 26degree and the average is 5.4degree. The difference between the predictive value and the calculated value is large when d/C_n=0.07. Thus it is necessary to improve the expression of the prediction. From the above, it is clear that the effect of each interaction can be expressed using an exponential function or a power function, so the difference between the predictive value and the calculated value of the amplitude easily becomes large when d/C_n is small. Therefore, if the number of calculations is increased when d/C_n is small and the expression is made again, the accuracy of the prediction can be improved. From the above, it is clear that simple expressions are possible for the relation between the axial gap length and the unsteady force, the amplitude and the phase of unsteady force and this relation is different according to bucket height h and FT and FA.

Next, prediction of the nozzle-bucket axial gap length by which the unsteady force becomes an extreme value is considered. It is confirmed that the unsteady force becomes nearly the maximum value when the potential field and the wake interactions are in the same phase, and the unsteady force becomes nearly the minimum value when the potential field and the wake interactions are in opposite phases. The axial gap length that leads to the extreme value cannot be decided only by the phase, because the amplitude of each interaction changes with the axial gap length. When the value at which Eq. (3) is differentiated by d/C_n is 0, the axial gap length takes the extreme value. When d/C_n is replaced with x, the differential equation is expressed by:

$$\frac{dF(x)}{dx} = ab \cdot e^{bx} \sin(k_p x + i_p + j) + ak_p \cdot e^{bx} \cos(k_p x + i_p + j) + mnx^{n-1} \sin(k_w x + i_w + j) + mk_w x^n \cos(k_w x + i_w + j) \quad (7)$$

where a, b, m and n are the coefficients when the force of the potential field interaction is expressed by an exponential function shown by Eq. (8) and the force of the wake interaction is expressed by a power function shown by Eq. (9).

$$F_p(x,t) = a \cdot e^{bx} \sin(wt + \theta_p) \quad (8)$$

$$F_w(x,t) = m \cdot x^n \sin(wt + \theta_w) \quad (9)$$

And j in Eq. (7) is the phase when the unsteady force becomes the maximum and it is a function of $x=d/C_n$. The relation between j and θ is expressed by Eq. (10).

$$j(x) = 90 - \theta(x) \quad (10)$$

Figure 9 presents the results obtained by Eq. (7) which is useful to predict the axial gap length at extreme values of the unsteady force. The ordinate is normalized by dividing the value of Eq. (7) by the maximum value in the range of $0.0<d/C_n \leqq 0.4$. Figure 9 shows that the trend of the value of Eq. (7) to d/C_n is different

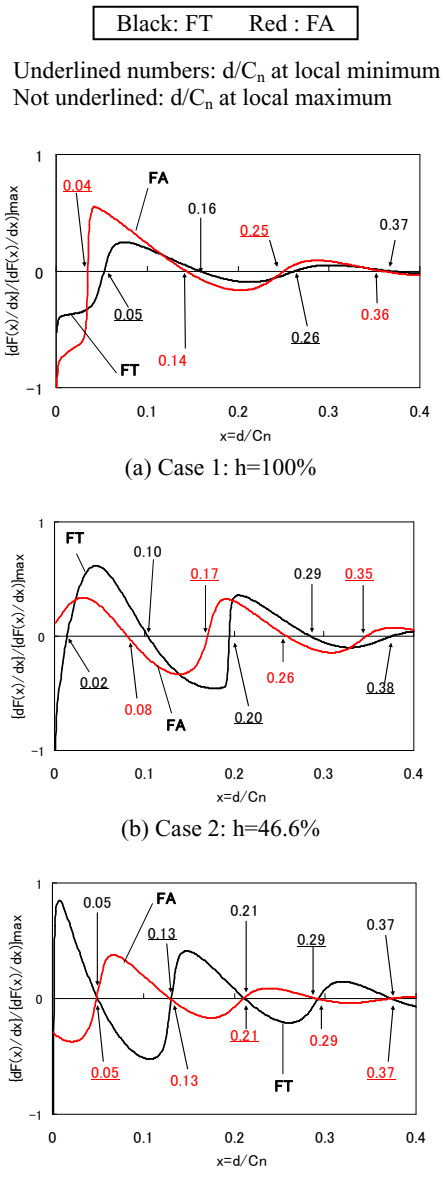

(a) Case 1: h=100%

(b) Case 2: h=46.6%

(c) Case 3: h=0%

Fig. 9 Prediction of axial gap length at an extreme value of the unsteady force

acording to bucket height h, namely there is a different bucket profile. When h is large, the value of d/C_n at the extreme values of the unsteady force is close for FT and FA, and there are only a few extreme values. The axial gap length that can reduce both FT and FA as much as possible can be selected easily for such h. But in case 3, where FT becomes the maximum, while FA becomes the minimum, there are a lot of extreme values compared with cases 1 and 2. Therefore, it is necessary for a bucket shape like that of case 3 to choose the axial gap length that does not enlarge the unsteady force. From the above, for bucket design, it is clearly important to get the tendency of the amplitude and the phase of each interaction quantitatively. It is confirmed that the axial gap length d that become extreme values obtained from Eqs. (1) and (7) are equivalence.

Next, the unsteady force obtained assuming that the potential field interaction and the wake interaction are in the same phase (shown in Fig.8) is considered. The unsteady force becomes large for FT when the axial gap length becomes small and bucket height h is small. But the factor causing the unsteady force to become large differs according to bucket height h. In case 2, the factor is the effect of the potential field interaction, but in case 3, the factor is the effect of the wake interaction. FA shows hardly any difference for the unsteady force with bucket height h.

Finally, the amplitude of each interaction is considered. The amplitude of the effect of the potential field interaction is largest in case 2, it does not depend on FT and FA. But the amplitude of the effect of the wake interaction is largest in case 3 for FT, and in case 1 for FA, thus the trend of the amplitude of each interaction is different. Moreover, the effect of the wake interaction for FT in case 3 is extremely large compared with the other cases, so it is necessary for generalization of the unsteady force to study the factor related to the difference of the effect by bucket height h.

As exemplified by the results of the generalization of the unsteady force, the present numerical method is effective for designing a turbine bucket with reduced stress on the bucket, so it is useful to produce highly reliable turbomachines.

CONCLUSIONS

The unsteady force of steam turbine buckets was examined by 2-dimensional CFD. The split method was described which examined the effect of the potential field interaction and the wake interaction from a viscous field that complexly affects the unsteady force. The method does two computations for one model to get inviscid and viscous flow solutions. For the unsteady inviscid flow (Euler) solution, using a sharply pointed shape (cusp) for the nozzle trailing edge instead of the actual round shape is the key to restrain the dummy wake generation. Then only the potential field interaction can be obtained. The unsteady force acting on the bucket obtained from the U-RANS consists of both potential field and wake interactions effects. Assuming a linear relation between potential field and wake interactions, the unsteady force induced by the wake interaction is obtained by subtracting the Euler's aero-dynamic force from that of the U-RANS.

This paper adopted the nozzle-bucket axial gap length for the factor to be studied and used the proposed method to calculate the unsteady force of the bucket sections with different bucket heights in the same stage. Three points were seen from these results. (1) The amplitude of the unsteady force with the nozzle passing frequency component could be approximated by an exponential or a power function of the axial gap length. (2) The absolute value of the effect from each interaction was different due to the bucket section difference. (3) The phase of the unsteady force with the nozzle passing frequency component fluctuation had a linear relationship with axial gap length. As a result of this linearity, a simple expression was possible for the relationship between the nozzle-bucket axial gap length and the unsteady force and between the amplitude and the phase of unsteady force with the nozzle passing frequency component. The unsteady force obtained from the simple expressions showed good agreement with results of viscous flow computation.

In conclusion, the proposed simple relationships between the nozzle-bucket axial gap length and the unsteady force were effective and easily predicted the force.

REFERENCES

[1] Lan, J., Xie, Y., and Zhang, D., 2008, "Study on Unsteady Aerodynamic Force of Turbine Blade with Different Mass Flow," *Proceedings of POWER 2008*, POWER2008-60157, pp. 341-347.

[2] Praisner, T. J., Grover, R., Mocanu, R., and Gacek, R., 2010, "Predictions of Unsteady Interactions between Closely Coupled HP and LP Turbines with Co- and Counter-Rotation," *Proceedings of ASME Turbo EXPO 2010*, GT2010-23681, pp. 1-10.

[3] Kemp, N. H., and Sears, W. R., 1955, "The Unsteady Forces Due to Viscous Wakes in Turbomachines," *Journal of the Aeronautical Sciences*, Vol. 22, pp. 478-483.

[4] Osborne, C., 1972, "Compressible Unsteady Interactions between Blade Rows," *AIAA Journal*, Vol. 11(3), pp.340-346.

[5] Naumann, H., and Yeh, H., 1973, "Lift and Pressure Fluctuations of a Cambered Airfoil under Periodic Gusts and Applications in Turbomachinery," *ASME Journal of Engineering for Power*, Vol. 95(1), pp.1-10.

[6] Nishiyama, T., and Funazaki, K., 1989, "Aerodynamic Interactions between the Steady Cascade Loading and Inflow Gust Vorticity (Vorticity Effect in Turbine Rotor Cascade)," *Transactions of the Japan Society of Mechanical Engineers*, Vol. 55(510), pp.306-312.

[7] Korakianitis, T., 1992, "On the Prediction of Unsteady Forces on Gas Turbine Blades: Part 1 – Description of the Approach," *Transactions of the ASME*, Vol. 114, pp.114-122.

[8] Korakianitis, T., 1992, "On the Prediction of Unsteady Forces on Gas Turbine Blades: Part 2 – Analysis of the Results," *Transactions of the ASME*, Vol. 114, pp.123-131.

[9] Feiereisen, J. M., Montgomery, M. D., and Fleeter, S., 1993, "Unsteady Aerodynamic Forcing Functions: A Comparison between Linear Theory and Experiment," *The American Society of Mechanical Engineers*, 93-GT-141, pp.1-12.

[10] Goldstein, M. E., 1978, "Unsteady Vertical and Entropic Distortions of Potential Flows Round Arbitrary Obstacles," *Journal of Fluid Mech.*, Vol. 89(3), pp.433-468.

[11] Jocker, M., Hillion, F. X., Fransson, T. H., and Wahlen, U., 2002, "Numerical Unsteady Flow Analysis of a Turbine Stage with Extremely Large Blade Loads," *ASME Journal of Turbomachinery*, Vol. 124, pp.429-438.

[12] Hoyningen-Huene, and M. V., Hermeler, J., 1999, "Time-Resolved Numerical Analysis of the 2-D Aerodynamics in the First Stage of an Industrial Gas Turbine for Different Vane-Blade Spacings," *The American Society of Mechanical Engineers*, 99-GT-102, pp.1-12.

[13] Roe, P. L., 1986, "Characteristic-Based Schemes for the Euler Equations," *Annual Review of Fluid Mechanics*, Vol. 18, pp.337-365.

[14] Chien, K. Y., 1982, "Predictions of Channel and Boundary-Layer Flows with a Low-Reynolds-Number Turbulence Model," *AIAA Journal*, Vol. 20(1), pp.33-38.

[15] Launder, B. E., and Spalding, D. B., 1974, "The Numerical Computation of Turbulent Flows," *Computer Methods in Applied Mechanics and Engineering*, Vol. 3(2), pp.269-289.